Optim Eng (2016) 17:813–832
DOI 10.1007/s11081-016-9321-6

# Stope optimization with vertical convexity constraints

**Gonzalo Nelis**[1] · **Michel Gamache**[2] · **Denis Marcotte**[3] · **Xiaoyu Bai**[3]

Received: 8 March 2015 / Revised: 1 January 2016 / Accepted: 13 March 2016 /
Published online: 4 May 2016


**Abstract** A new algorithm for the optimal stope design problem is proposed. It is based on a previous methodology developed by Bai et al. (Comput Geosci 52:361–371, 2013a) where a cylindrical coordinate system is used to define geomechanical restrictions and to find the optimal stope around an initial raise. The new algorithm extends this work using an integer programming formulation and a new set of constraints, aimed to solve geomechanical issues present on the original methodology. The new formulation is tested on two synthetic and one real deposits. An economic, geomechanical and feasibility analysis is performed, comparing the new results with Bai's methodology. This methodology achieves better stope designs in terms of geomechanical stability and wall regularity, generating feasible stopes for real use. It also allows further extensions to incorporate other geometrical constraints in order to obtain more regular stope designs.

**Keywords** OR in mining · Stope optimization · Underground mining · Sublevel stoping

✉ Gonzalo Nelis
gnelis@ing.uchile.cl

[1] Department of Mining Engineering, Delphos Mine Planning Laboratory and Advanced Mining Technology Center, University of Chile, Av. Tupper 2069, 8370451 Santiago, Chile

[2] GERAD Research Center and Department of Mathematics and Industrial Engineering, École Polytechnique, P.O. Box 6079, Station Centre-Ville, Montreal, QC H3C 3A7, Canada

[3] Department of Civil, Geological and Mining Engineering, École Polytechnique, P.O. Box 6079, Station Centre-Ville, Montreal, QC H3C 3A7, Canada

## 1 Introduction

The main objective of underground mining is to achieve the highest profit from the orebody while maintaining a safe operation. To achieve this, both economical and geomechanical factors have to be considered for the selection of the mining method and the design of the associated stopes. One of the most widespread underground mining systems is "Sublevel Stoping", in which an open stope is created with dimensions according to geomechanical conditions of the rock mass, the selectivity desired and profitability of the stope. Figure 1 shows a scheme of this method.

Several methods have been proposed to address the underground design problem and they can be classified in 1D, 2D and 3D methods. Among the 1D and 2D methods, the most relevant are the dynamic programming algorithm (Riddle 1977) and the branch and bound technique (Ovanic and Young 1995), which find the optimal design but they do not consider the three dimensional nature of the problem. On the other hand, the most relevant 3D methods are the floating stope algorithm (Alford 1996), the octree division algorithm (Cheimanoff et al. 1989), the maximum value neighborhood method (Ataee-Pour 2000), and simulated annealing techniques (Manchuk and Deutsch 2008). All these methods address the three dimensions, but they cannot incorporate real geomechanical restrictions in their formulation. Some

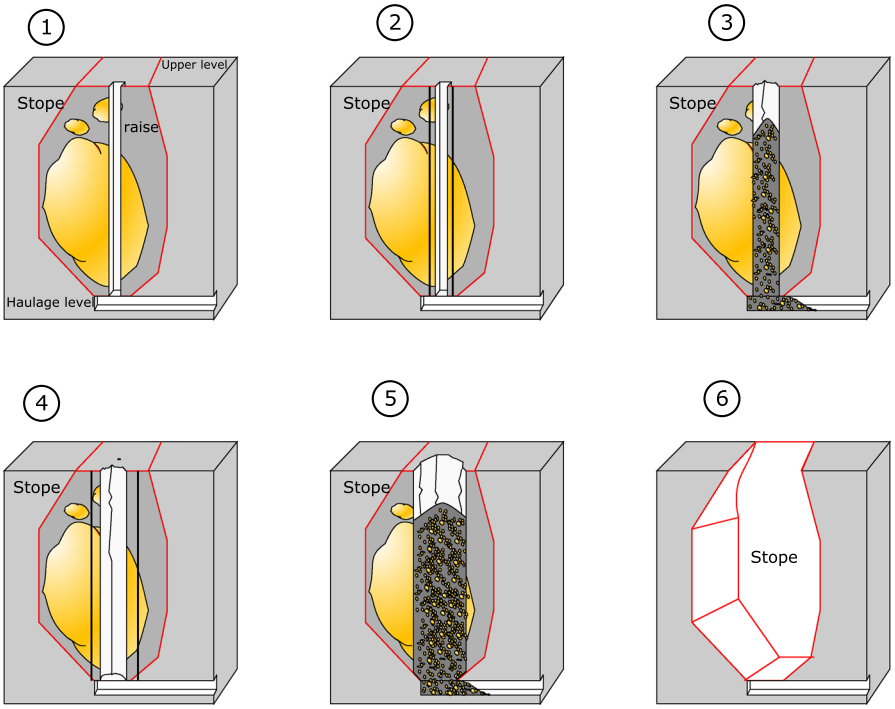


**Fig. 1** A scheme of the sublevel stoping method. The different figures show the progression from the initial raise and the ore blasting to the final open stope

of these methods may incorporate an additional step to test the stability of the current solution in order to generate stable designs, but they cannot address the geomechanical restrictions directly. A comprehensive review about these methods can be found in Ataee-Pour (2005).

Other methodologies are based on evaluating different locations of predefined stopes to find the best global layout. Topal and Sens (2010) propose an algorithm to find the optimum stope layout based on different possible stope sizes and using the economic value of these stopes to choose the best layout. However this methodology only generates a single mine layout when the optimum must be chosen from all the possible layouts for the given stope sizes. Sandanayake et al. (2015) address this issue with a heuristic approach which considers a set of possible stope layouts to find the optimum. However, this approach still depends on the initial stope sizes used in the algorithm and does not consider the rock pillars between stopes.

Recent progress have been made on this subject for the case of sublevel stoping. In Bai et al. (2013a), the authors find the stope design that maximizes the profit obtained. Their approach is based on a transformation from the Cartesian coordinate system to a cylindrical system centered around the initial raise. The authors could define the optimal stope incorporating some geomechanical constraints as the footwall and hangingwall angles, the minimum stope width that ensures the flow of the blasted ore towards the raise, and the maximum distance from the raise to control the size of the final stope. This approach was extended to include multiple raises (Bai et al. 2014) and to incorporate drift development in the optimization process (Bai et al. 2013b). This problem can be solved using a network structure and an efficient maximum flow algorithm (Picard 1976).

In deposits with regular geometries, with a homogeneous grade distribution, this methodology generates feasible stope designs. However, on irregular deposits, with scattered mineralization, the stope designs may present stability problems with irregular contours, despite the imposed restrictions of footwall and hangingwall angles.

The stope stability is defined based on the rock mass properties such as uniaxial or triaxial compressive strength, rock mass condition, presence of faults or structures, etc. (Bieniawski 1989; Laubscher 1990). To ensure the stability of a given stope it is necessary to define its shape, maximum dimensions, footwall and hangingwall angles and the global stope inclination (Mathews 1980). The methodology proposed by Bai successfully incorporates the footwall and hangingwall angles and the stope maximum dimensions, but in some cases the stopes present shapes that reduce their global stability. Figure 2 illustrates such a stope obtained with Bai's approach where stability problems may occur, resulting in increased ore dilution. This dilution comes from the walls of the stope in its midsection, where a failure may occur given its non-convex shape, depending on the quality of the rock mass. If the wall rock is blocky, with multiple sets of joints and with poor surface quality (GSI lower than 40 according to Hoek et al. 2002), the cohesion between this section and the wall rock will be low, so the failure probability would be high. The quality of the blasting will also affect the probability of failure of this section: a poor blasting technique will damage the surrounding

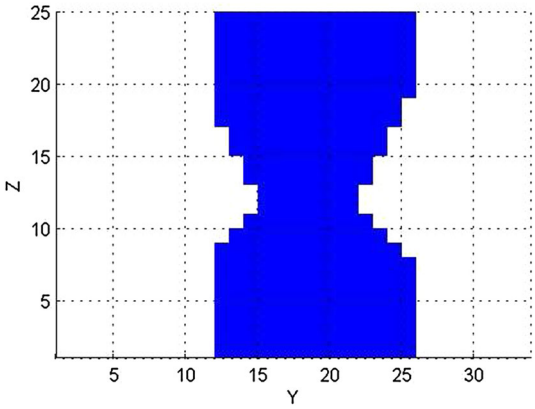


**Fig. 2** Stope generated by Bai's methodology, with stability issues. The stope is 12 m wide and 25 m tall approximately. *YZ* vertical section at X = 30

walls of the stope, decreasing the strength of the wall rock and therefore, increasing the probability of failure. Furthermore, a high horizontal stress condition will generate a tension zone in this section with a negative impact on its stability. Given this scenario, a methodology which fulfills the maximum stope dimensions and also avoids this kind of geometries would be useful for some rock mass and mining conditions.

In the next section, we briefly review the method used to measure stope stability. We show how the lack of convexity along the stope sides influence negatively the stability. We recall the main points of the approach used by Bai et al. (2013a). Then we describe the new linear program used to enforce a particular form of convexity of the stopes in the vertical direction. Finally, the results obtained with and without the convexity constraints are compared on a few simple synthetic deposits and a real deposit.

## 2 Methods

### 2.1 Stope stability determination

To study the stope stability, we use the strength factor defined as:

$$\mathrm{SF} = \frac{\text{Rock mass strength}}{\text{Induced stress}}. \tag{1}$$

Figure 3 presents the SF obtained from a 2D stability analysis of the stope central cross-section.

The analysis is done using Examine2D (Roclab, 2014). The software implements 2D boundary elements analysis (Crouch and Starfield 1983) to calculate the stress induced in the rock mass around the excavation. It assumes a linear, elastic, continuous, isotropic and homogeneous rock mass and, of course, it neglects the third dimension. Despite these strong assumptions and simplifications, the stability

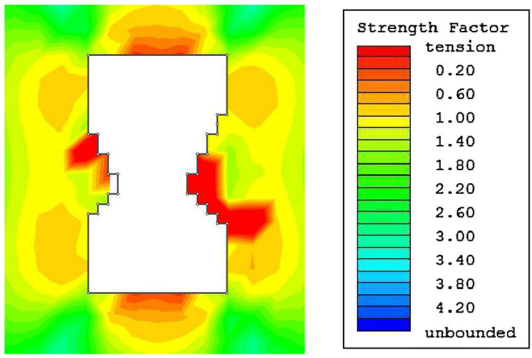


**Fig. 3** Stability analysis of stope generated by Bai's methodology, with stability issues. The *midsection* presents possible failure by tension

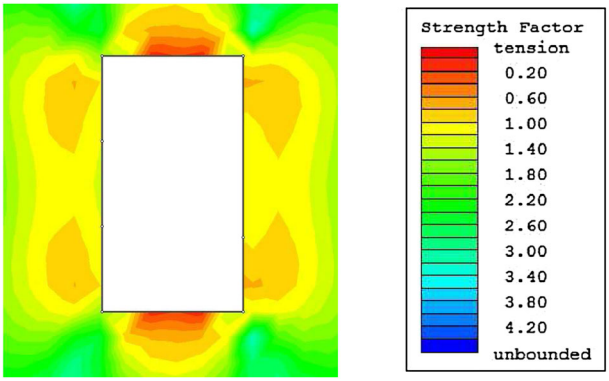


**Fig. 4** Stability analysis of a stope with the same dimensions as Fig. 3, but with a *straight midsection*. The previous tension zone presents a better stability

analysis remains useful to compare relative stability of different stope designs in a given rock mass.

For simplicity, the failure criterion to calculate SF was Mohr–Coulomb (Coulomb 1776), but any other failure criterion could be used. The midsection presents a possible failure by tension zone. This section will flow inside the stope, diluting the ore and reducing the stope profit. Hence, this design could be not optimal when considering the additional dilution. For comparison, a stope with the same dimensions is presented in Fig. 4 but with a straight midsection.

## 2.2 Model formulation

The proposed model is based on the ultimate pit problem or final pit problem in open pit mining (Lerchs and Grossmann 1965). The objective is finding the part of the orebody which maximizes the profit obtained when it is extracted and processed. To achieve this objective, the original orebody is discretized in small blocks with different attributes such as metal content, extraction cost, processing cost, tonnage,

coordinates, etc. From these attributes, an economic block model is defined using a profit function (Lane 1988), where each block has a value representing the net profit of extracting that particular block. It is important to mention that the set of blocks extracted must ensure the pit wall stability, typically defined as a wall pit angle. For this reason, geometrical precedence constraints are defined between blocks to maintain the required angle. Formally, this problem can be defined as a linear integer program (IP; Lerchs and Grossmann 1965):

$$\max \sum_{i \in N} x_i p_i, \tag{2}$$

$$\text{s.t. } x_i \leq x_j \quad \forall (i, j) \in \mathcal{P}_i, \tag{3}$$

$$x_i \in \{0, 1\} \quad \forall i \in N. \tag{4}$$

The variable $x_i$ equals 1 if the block $i$ in $N$ is extracted and 0 otherwise. The parameter $p_i$ is the extracting value of block $i$. The restriction set is derived from the precedence constraints between blocks to maintain the wall pit angle. The set $\mathcal{P}_i$ contains all ordered pairs $(i, j)$ where block $j$ must be extracted before block $i$. Finally, the objective is to find the set of blocks that maximizes the profit, subject to every block in this set must be extracted towards the surface fulfilling the precedences between blocks.

Similarly, in the sublevel stoping mining system, a vertical raise is drilled in order to create enough space to blast the ore inside the stope. The blasted material fills the raise and falls down by gravity towards the drawpoints located in the bottom of the stope. Sequential blasts are performed to extract all the material in the stope taking advantage of the new space created from former blasts. Therefore, the role played by this initial raise is analogous to the surface in open pit mining: all the blocks must move towards the raise/surface in order to be extracted. Hence, the precedences between blocks should link every block to the initial raise. This is the base for the cylindrical coordinate system transformation proposed by Bai et al. (2013a).

### 2.3 Cylindrical block model

In Bai et al. (2013a), an algorithm to transform a conventional block model (in the Cartesian coordinate system) into a cylindrical block model is proposed in order to emulate the role played by the ground surface in open pit mining with the initial raise in sublevel stoping. The raise is defined as the center of the cylindrical system, and a set of regular blocks are defined surrounding this raise from a discretization of $\Delta r$, $\Delta\theta$ and $\Delta z$ defined by the user. This transformation presents a big advantage: to extract any block of the block model, diagonal links can be defined in the cylindrical system towards the raise, and this structure of links can be represented in the three-dimensional space to generate the geometry shown in Fig. 5.

This figure shows that any block to be extracted forces all its predecessors towards the raise to be extracted too, emulating the desired behavior. Furthermore,

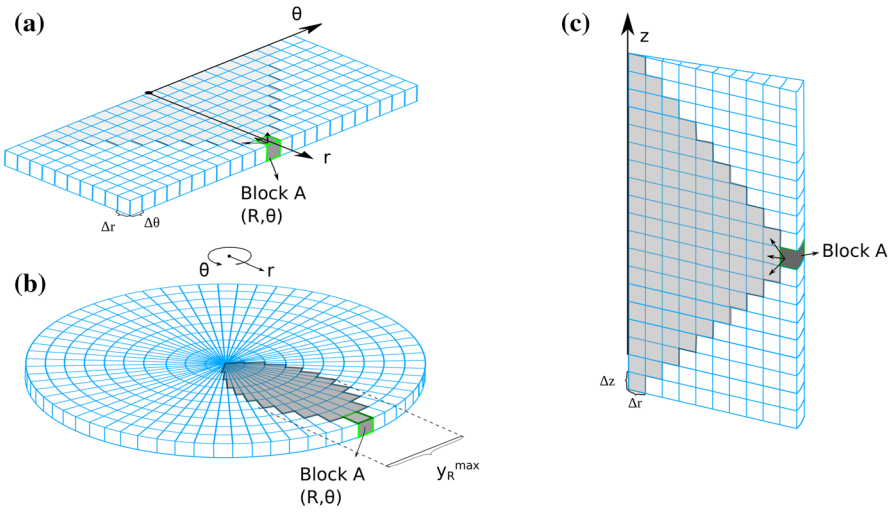


**Fig. 5** Illustration of the cylindrical coordinate system; **a** *horizontal* precedences in the ($r$, $\theta$) plane, **b** the same blocks as in **a** shown in their real spatial position, and **c** precedences in the *vertical plane* to generate the footwall and hangingwall constraints. *Shaded blocks* are the *blocks* to remove to extract *block A*. *Black point* in the *center* represents the raise

using this transformation, the footwall and hangingwall angles can be defined directly with diagonal links as shown in Fig. 5c. Also, the discretization of $\Delta r$, $\Delta\theta$ and $\Delta z$ can be chosen based on the footwall and hangingwall angles and the stope width parameter ($y_R^{max}$) to allow a steady flow of material towards the raise. This problem can be solved using a network structure and efficient maximum flow or other algorithms. After solving the problem in the cylindrical system, a back-transformation is necessary to get the optimum stope design in terms of the original (Cartesian) block model.

In this paper we will use the same transformation proposed by Bai et al. (2013a), with the same precedences of footwall and hangingwall angles and the minimum stope width. The raise location is considered known, but it can be optimized as in Bai et al. (2014). This is the base used to improve the algorithm with the new constraints presented in the next section.

### 2.4 Stope convexity constraints

It is not possible to avoid the irregular shapes in the stope outer section by imposing vertical upward and downward precedences between blocks in the cylindrical coordinate system as this would impose to take the entire column of blocks as soon as a block is part of the stope. For this reason, the restriction must be imposed in a different way. In Fig. 6a, a single column from a block model is presented. To avoid non-convex geometries in the vertical direction, we must consider that if a block from this column is extracted, and the block immediately below is not, then all the blocks below must not be extracted. Equivalently, if a block is extracted and the block immediately above is not, then all the blocks above must not be extracted. For

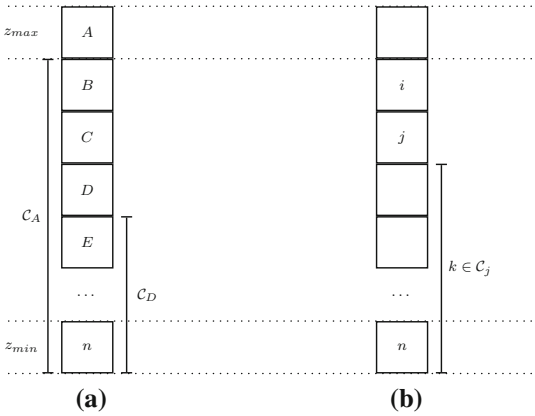


**Fig. 6** A single column of a block model

instance, if block A is extracted and block B is not, all the blocks below B must not be extracted in order to avoid the generation of non-convex geometries. The advantage of putting the restrictions in this way is that it does not interfere with either the footwall or the hangingwall constraints because it does not force the vertical extraction in all situations. Note that in the horizontal plane, the stope can be non-convex. However, this is not expected to cause any potential stability problems. Although it is possible to enforce full convexity, this is not attempted here as it would constrain the solutions to unrealistically smooth stopes perfectly symmetric around the raise. Hereafter, we use the term convexity as a shortcut for vertical convexity.

For the implementation of this restriction, let define $\mathcal{N}$ the set of blocks. Let $\mathcal{N}^T = \{i \in \mathcal{N} | z_i = z_{max}\}$ be the set of all blocks located on the top level of the block model and similarly let $\mathcal{N}^B = \{i \in \mathcal{N} | z_i = z_{min}\}$ be the set of all blocks located on the bottom level of the block model. Let define a column as the set of all blocks with the same $r$ and $\theta$ coordinates, or the same $x$ and $y$ coordinates in the Cartesian system. Let $\mathcal{C}_i = \{j \in \mathcal{N} \mid r_i = r_j,\ \theta_i = \theta_j, \text{ and } z_i > z_j\}$ be the set of all blocks below the block $i$ in a single column. Finally, let $\mathcal{C}_i^1 = \{j \in \mathcal{C}_i \mid z_j = z_i - \Delta z\}$ be the set that includes only the block located immediately below $i$ in $\mathcal{C}_i$ (e.g., in Fig. 6a, $\mathcal{C}_A^1 = \{B\}$). With these definitions, the IP to force convexity is shown:

$$\begin{aligned} &\max \sum_{i \in N} p_i x_i \\ &\text{s.t.}\, x_i \leq x_j \quad \forall (i,j) \in \mathcal{P}_i, \end{aligned} \tag{5}$$

$$x_j + \alpha_j \geq x_i \quad \forall i \in \mathcal{N} \backslash \mathcal{N}^B, \quad j \in \mathcal{C}_i^1, \tag{6}$$

$$x_k \leq 1 - \alpha_j \quad \forall j \in \mathcal{N} \backslash \mathcal{N}^T, \quad \forall k \in \mathcal{C}_j, \tag{7}$$

$$x_i,\ \alpha_i \in \{0,\ 1\} \quad \forall i \in \mathcal{N}. \tag{8}$$

The decision variable $x_i$ equals 1 if the block $i \in \mathcal{N}$ is extracted and 0 otherwise, and the coefficient $p_i$ is its extracting value. In constraint (6), $j$ represents the block

immediately below $i$ in the block model (see Fig. 6b). The new binary variable $\alpha_j$ equals 1 if all the blocks $k \in \mathcal{C}_j$ *must not* be extracted and 0 otherwise (i.e., they can be extracted).

To clarify this concept, an example using Fig. 6a is shown where block $C$ is extracted (i.e., $x_C = 1$) and $D$ is not ($x_D = 0$). Applying these restrictions to the block $C$ in this column :

$$x_D + \alpha_D \geq x_C, \tag{9}$$

$$x_k \leq 1 - \alpha_D \quad \forall k \in \mathcal{C}_D = \{E, \ldots, n\}. \tag{10}$$

In this case, if block $C$ is extracted, and at the same time, $D$ is not extracted, restriction (9) forces the variable $\alpha_D$ to be 1. If this variable is 1, the right side in restriction (10) is 0, forcing all the blocks $k \in \mathcal{C}_D$ to be 0, or, in other words, all the blocks below $D$ must not be extracted (i.e., $x_E = 0, \ldots, x_n = 0$). Both restrictions combined avoid the non-convexity issues presented before, ensuring a better stope shape.

Let's now consider the blocks above a certain block. For example, let's consider that block $D$ is extracted. This necessarily means that $\alpha_C = \alpha_B = \alpha_A = 0$ (i.e., all the $\alpha$ associated with the blocks above $D$) according to constraint (7). On the other hand, constraint (6) for the blocks above $D$ are shown as follows:

$$x_C + \alpha_C \geq x_B, \tag{11}$$

$$x_B + \alpha_B \geq x_A. \tag{12}$$

If block $C$ is not extracted, the left side of restriction (11) equals 0, forcing $x_B$ to be 0 as well. In consequence, the left side of restriction (12) is also 0, forcing $x_A$ to be 0 as well. The propagation of this restriction forces all the blocks above $D$ to not be extracted in this example.

Both restrictions combined avoid the non-convexity issues presented before, ensuring a better stope shape. However, the addition of these new constraints with the new variable to the original problem generates the loss of the network structure. This structure is based on the fact that the restriction set must have only precedence constraints in the form of restriction (5), with only two variables for each restriction. The new constraints do not have this structure, therefore, this problem can not be solved using maximum flow algorithms. Branch and bound algorithms will be used instead, in order to find the optimum stope design. These algorithms are slower than maximum flow algorithms, hence the runtimes of this new problem will be studied as well.

## 3 Results

### 3.1 No convexity constraints

First of all we present the results obtained from the integer program implementation (IP-formulation) without convexity constraints solved with simplex and branch and bound algorithm implemented in Gurobi 5.6.3. This problem is equivalent to the

network problem solved by Bai with the maximum flow algorithm. Therefore, in order to validate the new implementation, we will compare the performance of both algorithms solving the same instance. A real orebody, presented in Fig. 7, will be used with the economical and geomechanical parameters shown in Table 1. The orebody is located in Canada [commodity (a metal) and exact location are undisclosed for confidentiality reasons]. It has been the object of a resource estimate report (NI-43-101) and could eventually be exploited by sublevel stoping.

Also, with the aim to test the performance in bigger instances, the cylindrical block model discretization $\Delta r/\Delta x$ was changed, where $\Delta x$ is the original block size in the $x$ direction. Changing this value generates different instances with different sizes as the number of blocks in the discretized cylindrical system equals the number of variables for the instance without convexity constraints. The performance of both algorithms is presented in Table 2.

As shown in Table 2, both methods achieve the same results in every field. Note that the small differences between the objective functions (profits in the cylindrical system) and the stope profits (profits in the Cartesian system) are due to the back-transformation to the Cartesian coordinates required for mining. The stope shape is also the same in both algorithms, as it can be seen in Fig. 8. With these results, we validate the IP implementation of Bai's methodology.

On the other hand, if we compare the runtime of the two algorithms, the maximum flow implementation solves the same instances up to four times faster than Gurobi. However, for the integer nature of this formulation, the results obtained by Gurobi are notably fast. This is due to the structure of these linear IPs: the restriction matrix generated by all the precedence constraints is totally unimodular. Therefore, the linear relaxation of these instances, solved by simplex, generates an integer solution without using the branch and bound techniques. This property causes a runtime

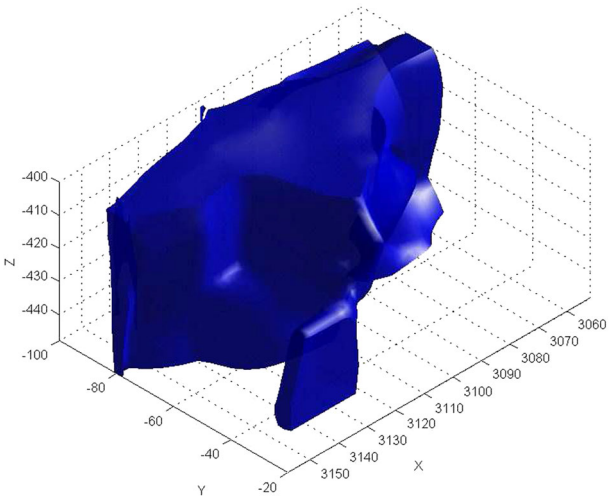


**Fig. 7** Real deposit used in this analysis

**Table 1** Geomechanical, design and economic parameters for stope optimization algorithm

| Parameters | Real deposit | Deposit 1 | Deposit 2 |
|---|---|---|---|
| Design and geomechanical parameters | | | |
| Minimum stope width (m) | 6 | 6 | 6 |
| Minimum footwall angle (°) | 60 | 63 | 60 |
| Minimum hangingwall angle (°) | 45 | 63 | 45 |
| Economic parameters | | | |
| Unitary cost ($/t) | 50 | 50 | 50 |
| Cut-off grade | 0.005 | 0.005 | 0.005 |
| Selling price ($/kg) | 10 | 10 | 10 |
| Recovery rate (%) | 90 | 90 | 90 |
| Density (t/m$^3$) | 2.3 | 2.3 | 2.3 |

**Table 2** Comparison between network structure: flow algorithm and IP formulation—Gurobi simplex algorithm

| $\Delta r/\Delta x$ | Algorithms | Objective function (k$) | Stope profit (k$) | Missed ore (k$) | Dilution (%) | Runtime (s) |
|---|---|---|---|---|---|---|
| 1 | Flow | 1184.27 | 1202.24 | 179.84 | 4.83 | 23.15 |
| | Gurobi | 1184.27 | 1202.24 | 179.84 | 4.83 | 69.87 |
| 0.5 | Flow | 1150.78 | 1196.60 | 187.68 | 3.57 | 43.06 |
| | Gurobi | 1150.78 | 1196.60 | 187.68 | 3.57 | 148.43 |
| 0.3 | Flow | 1145.03 | 1199.63 | 184.16 | 3.68 | 97.78 |
| | Gurobi | Out of memory error | | | | |

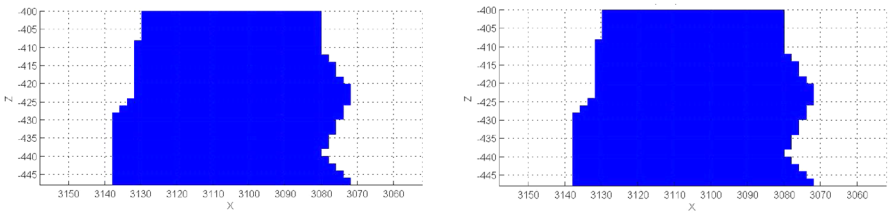


**(a)** Maximum flow **(b)** Gurobi

**Fig. 8** *Vertical* sections (Y = -68) of optimal stopes generated by maximum flow algorithm and Gurobi simplex algorithm after back-transformation to Cartesian coordinates

remarkably low compared to other instances with comparable size. Thereby, the IP-formulation is still useful for solving these instances.

## 3.2 Convexity constraints

To study the effect of the convexity constraints proposed before, three different orebodies were used. The first one corresponds to the real deposit used in the

**Table 3** Stope design results of IP-formulation for real deposit

| $\Delta r/\Delta x$ | Cases | Stope profit (k$) | Missed ore (k$) | Dilution (%) |
|---|---|---|---|---|
| 1 | No convexity | 1202.24 | 179.84 | 4.83 |
| | Convexity (gap 0.1 %) | 1200.86 | 180.15 | 5.39 |
| | Convexity (gap 0.01 %) | 1200.87 | 181.08 | 4.93 |
| 0.9 | No convexity | 1200.73 | 181.60 | 4.52 |
| | Convexity (gap 0.1 %) | 1198.72 | 182.57 | 5.14 |
| | Convexity (gap 0.01 %) | 1199.70 | 182.49 | 4.57 |
| 0.8 | No convexity | 1195.73 | 186.82 | 4.42 |
| | Convexity (gap 0.1 %) | 1194.41 | 187.39 | 4.84 |
| | Convexity (gap 0.01 %) | 1194.53 | 188.05 | 4.45 |

*No convexity* IP-formulation without convexity constraints, *Convexity* (*gap 0.1 %*) IP-formulation with convexity constraints. Minimum optimality gap: 0.1 %, *Convexity* (*gap 0.01%*) IP-formulation with convexity constraints. Minimum optimality gap: 0.01 %

previous section, presented in Fig. 7, and its results with the convexity constraints are presented in Table 3 along with the results obtained using Gurobi on the same instance without the new constraints, to compare both results graphically and quantitatively. In terms of value, for this orebody, the difference between both cases is less than 1 %, with a small raise in the dilution inside the stope, and less ore recovery. This behavior is expected due to the fact that the new constraints reduce the feasible region of the initial problem.

In relation to runtimes of both algorithms, the addition of the new constraints generates a significant increase of the solving time for the same deposit. This is due to the fact that the restriction matrix is not totally unimodular under the new constraints, therefore the simplex solution is not integer and branch and bound techniques must be applied, with the notable increase in the delivering time of the optimum stope, being up to 20 times slower than the original formulation. In this regard, it is pertinent to emphasize the magnitude of these instances in terms of variables and constraints (see Table 4). Compared to the original formulation, the number of variables is doubled as it is expected, due to the new $\alpha$ variable. Also, the number of constraints increases up to 3.2 times, generating an instance of nearly 3 millions of constraints with the smallest discretization presented here.

For the synthetic deposits, two different cases are shown. The first deposit represents an adverse case for the original algorithm since it contains high value on top and bottom zones, and a narrow band in its center (Fig. 9a). This geometry generates a non-convex zone in its midsection. The second case, shown in Fig. 9b, represents a deposit with scattered high grade blocks through all the orebody, producing irregular contours. The results for both orebodies are presented in Table 5.

For both cases, the addition of the convexity constraints lowers the stope profit, which is a expected result. This effect is different for each deposit: The first deposit presents the more adverse case for the convexity constraints, with a loss of 14 % in the stope profit and a dilution increase from 4.49 to 14.99 % for the smallest

**Table 4** Optimization results of IP-formulation for real deposit

| $\Delta r/\Delta x$ | Cases | Objective function (k$) | Optimality gap (%) | Constraints | Variables | Runtime (s) |
|---|---|---|---|---|---|---|
| 1 | No convexity | 1041.60 | – | 484,390 | 73,944 | 3.7 |
| | Convexity 0.1 | 1040.47 | 0.0631 | 1,337,590 | 147,888 | 45.4 |
| | Convexity 0.01 | 1040.95 | 0.0096 | 1,337,590 | 147,888 | 47.7 |
| 0.9 | No convexity | 1070.14 | – | 669,578 | 98,000 | 5.5 |
| | Convexity 0.1 | 1069.10 | 0.0511 | 1,992,578 | 196,000 | 128.6 |
| | Convexity 0.01 | 1069.28 | 0.0080 | 1,992,578 | 196,000 | 154.0 |
| 0.8 | No convexity | 1056.75 | 0 | 920,033 | 138,688 | 8.1 |
| | Convexity 0.1 | 1055.73 | 0.0522 | 2,935,343 | 277,376 | 229.4 |
| | Convexity 0.01 | 1056.15 | 0.0071 | 2,935,343 | 277,376 | 280.4 |

*No convexity* IP-formulation without convexity constraints, *Convexity 0.1* IP-formulation with convexity constraints. Minimum optimality gap: 0.1 %, *Convexity 0.01* IP-formulation with convexity constraints. Minimum optimality gap: 0.01 %

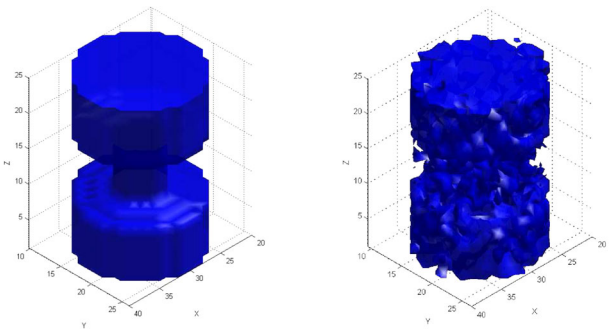

**(a)** Deposit 1 **(b)** Deposit 2

**Fig. 9** Isometric views of both synthetic deposits used in this analysis. Only blocks with positive profit value are shown

**Table 5** Stope design results of IP-formulation for synthetic deposits

| $\Delta r/\Delta x$ | Cases | Stope profit (k$) | Missed ore (k$) | Dilution (%) |
|---|---|---|---|---|
| Deposit 1 | | | | |
| 1.5 | No convexity | 340.77 | 42.43 | 8.41 |
| | Convexity (gap 0.5 %) | 305.09 | 40.39 | 17.77 |
| 1 | No convexity | 355.26 | 41.75 | 4.49 |
| | Convexity (gap 0.5 %) | 306.39 | 52.43 | 14.99 |
| Deposit 2 | | | | |
| 1 | No convexity | 984.27 | 33.14 | 23.01 |
| | Convexity (gap 0.5 %) | 947.33 | 47.50 | 30.23 |
| 0.9 | No convexity | 993.40 | 17.18 | 24.48 |
| | Convexity (gap 0.5 %) | 958.13 | 31.56 | 30.79 |

**Table 6** Optimization results of IP-formulation for synthetic deposits

| $\Delta r/\Delta x$ | Cases | Objective function (k$) | Optimality gap (%) | Constraints | Variables | Runtime (s) |
|---|---|---|---|---|---|---|
| Deposit 1 | | | | | | |
| 1.5 | No convexity | 373.78 | – | 20,600 | 3920 | 0.94 |
| | Convexity 0.5 | 324.97 | 0.47 | 34,712 | 7840 | 2.245 |
| 1.0 | No convexity | 359.41 | – | 64,308 | 11,760 | 2.86 |
| | Convexity 0.5 | 308.13 | 0.48 | 129,828 | 23,520 | 166.77 |
| Deposit 2 | | | | | | |
| 1 | No convexity | 949.80 | – | 142,608 | 21,840 | 6.17 |
| | Convexity 0.5 | 923.11 | 0.48 | 394,608 | 43,680 | 109.60 |
| 0.9 | No convexity | 965.85 | – | 195,118 | 28,644 | 7.42 |
| | Convexity 0.5 | 939.08 | 0.49 | 581,812 | 57,288 | 265.68 |

discretization ($\Delta r/\Delta x = 1$). The dilution increases since the solution must add new waste blocks to meet the new constraints. Regarding deposit 2, the profit loss is around 4 % with a small increase in dilution.

Moreover, it is relevant to mention that the addition of convexity constraints produces a greater amount of ore missed compared to the original solution in almost every instance. This can be interpreted as a trade-off between ore and value: in some zones of the deposit it is better to leave certain ore blocks out of the solution in order to meet the convexity constraints. Adding these extra ore blocks would add too much dilution to the solution.

The differences between the resolution time with and without convexity constraints vary greatly depending on the size of the problem (see Table 6). For the first deposit, for instance, with a discretization of $\Delta r/\Delta x = 1.5$, the runtime is almost tripled when convexity constraints are used. On the other hand, with a discretization of $\Delta r/\Delta x = 1.0$, the solving time is up to 58 times greater for the same deposit. This indicates the great impact of the instance size on the solving times. For example, despite being the same deposit, increasing the variables and constraints using a smaller discretization generates a solving time 2.5 times greater for the lowest gap shown in Table 6 for deposit 2: from 109.6 to 265.68 s.

### 3.3 Stope shape and stability

To study the stope stability on the new solutions, we compare different stope designs in Examine2D, showing the SF using Hoek and Brown (Hoek et al. 2002) and Mohr–Coulomb (Coulomb 1776) failure criteria according to the parameters and geomechanical conditions shown in Table 7. The results for the real deposit (Fig. 10) are presented in Fig. 11. Those for the synthetic deposit (Fig. 12) are presented in Figs. 13 and 14.

In Fig. 11, the original stope presented a non-convex zone in its corner, generating a failure by tension zone. The new stope, on the other hand, does not present that tension zone, achieving a greater stability in that corner. Furthermore,

**Table 7** Geomechanical and failure criterion parameters

| Parameters | Values |
|---|---|
| In situ stress parameters | |
| Depth (m) | 450 |
| Overburden unit weight (MN/m$^3$) | 0.026 |
| Horizontal stress ratio | 1.5 |
| Out of plane stress ratio | 1.2 |
| Rock mass strength parameters | |
| Tensile strength (MPa) | 0.3 |
| Cohesion (MPa) | 2 |
| Friction angle (°) | 50 |
| High quality rock | |
| Intact compact strength (MPa) | 250 |
| GSI | 75 |
| mi | 25 |
| Low quality rock | |
| Intact compact strength (MPa) | 100 |
| GSI | 30 |
| mi | 25 |

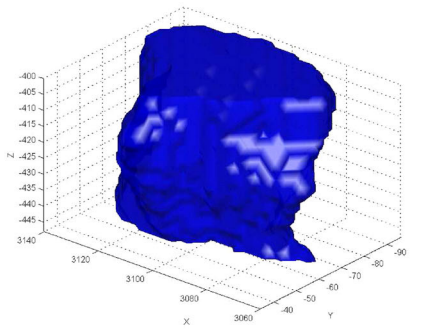

**(a)** Isometric without convexity constraints

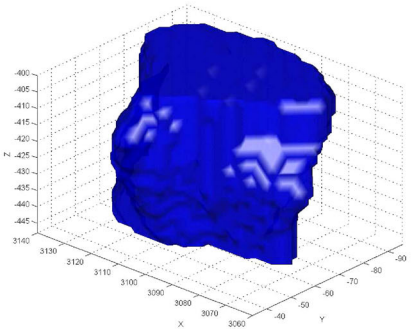

**(b)** Isometric with convexity constraints

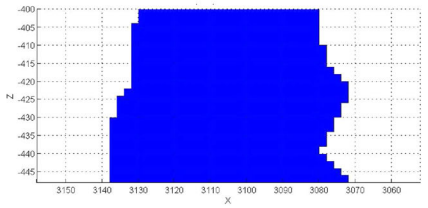

**(c)** Slice XZ (Y=-68) without convexity constraints

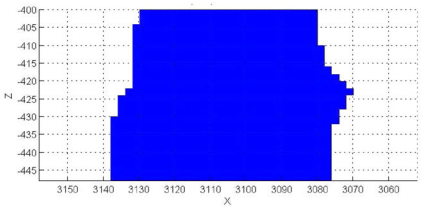

**(d)** Slice XZ (Y=-68) with convexity constraints

**Fig. 10** Stope shapes of both algorithms applied on real deposit

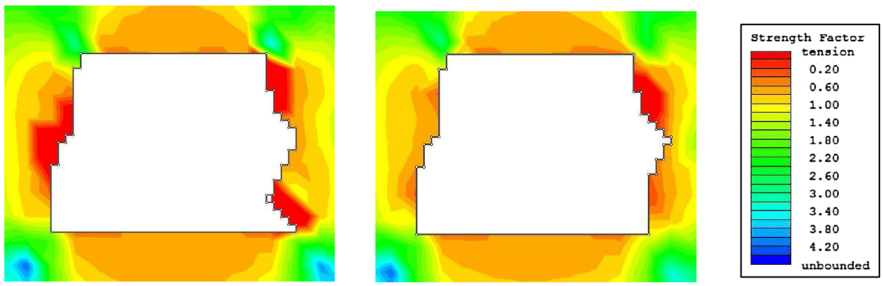


**(a)** Without convexity constraints **(b)** With convexity constraints

**Fig. 11** Stability analysis of a cross-section on real deposit stope

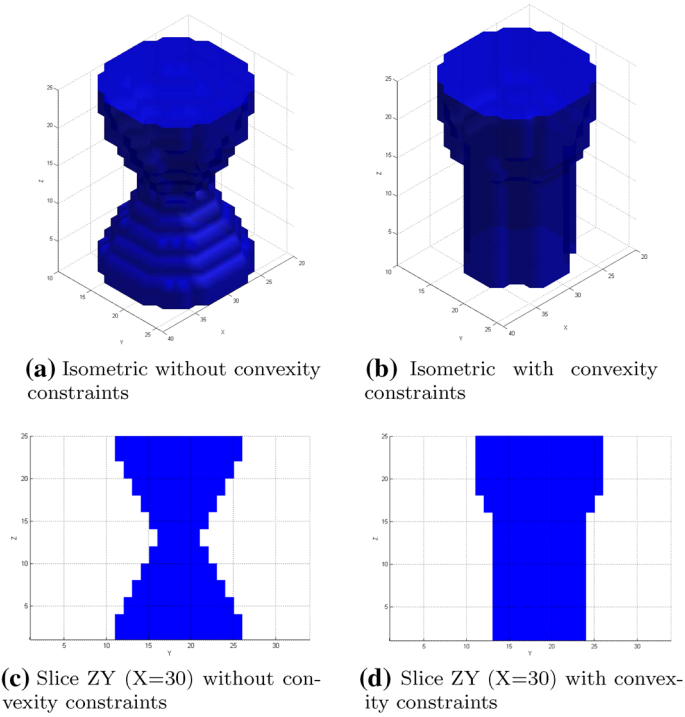

**(a)** Isometric without convexity constraints **(b)** Isometric with convexity constraints

**(c)** Slice ZY (X=30) without convexity constraints **(d)** Slice ZY (X=30) with convexity constraints

**Fig. 12** Stope shapes of both algorithms applied on deposit 1

the stope stability in other zones also improves as we can see in the upper-left corner, where the original stope had an unstable zone that was improved significantly with the new constraints. The induced stress over this zone changes due to the regularization of the stope. Therefore, the convexity constraints can improve not only the local stability, but the global stability as well.

Similar observations can be made for the synthetic deposit (Fig. 13). The failure zone in the mid-zone is substantially reduced with the new convexity constraints.

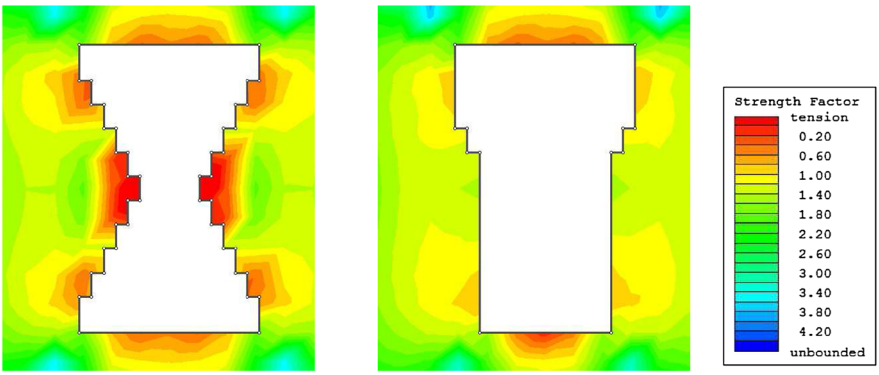


**(a)** Without convexity constraints **(b)** With convexity constraints

**Fig. 13** Stability analysis of a cross-section on synthetic deposit 1. High quality rock mass

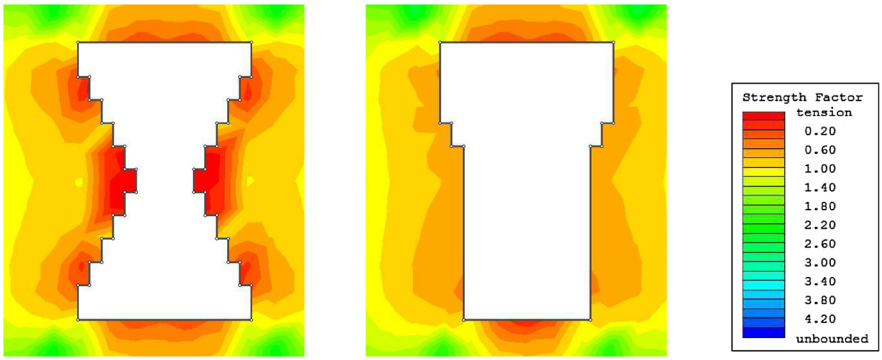


**(a)** Without convexity constraints **(b)** With convexity constraints

**Fig. 14** Stability analysis of a cross-section on synthetic deposit 1. Low quality rock mass

This behavior holds true for different rock mass qualities, as it can be seen in Fig. 14, where we evaluated the same stope geometry, under the same stress conditions, but with a low quality rock mass detailed in Table 7. Therefore, the new geometries generated by the convexity constraints are more stable than the stopes from the original methodology, independently of the rock mass quality.

## 4 Discussion

The new IP-formulation presented in this work improves the stope designs obtained by the network formulation by Bai et al. (2013a). The addition of the convexity constraints achieves more regular and geomechanically more stable shapes without

using an additional step to manually regularize the stope borders with the risk of loosing the design optimality.

In the examples presented, the stopes obtained under the new IP formulation are comparable with the stopes obtained by Bai's methodology, with differences that range from less than 1 to 13 % in the stope profit function. However, depending on the cost structure, the stope profit reduction could be greater with the IP formulation, since it forces to add waste blocks or to eliminate ore blocks from the original solution to fulfill the convexity constraints. These may be critical in low-grade deposits where a subtle change in the stope design may produce a great change in its profit.

It can be noticed, also, that the new constraints structure allows the solution to add or discard blocks from the original solution obtained by Bai's methodology, depending of the value generated by these actions. This is a clear advantage over a manual adjustment stage since it is not trivial to determine whether to add or subtract blocks to achieve a better geometry, while seeking the best possible value and respecting the diagonal precedence constraints to maintain the footwall and hangingwall angles.

Regarding stability, all the new designs are more stable than their previous solutions obtained without the constraints. However, there are still some areas with lower stability despite complying with all the restrictions imposed on the formulation. This can be solved by generating smaller stopes, modifying the stope height (controlled by the raise length in the original Bai's algorithm) and the stope length (controlled by the parameter $R$ in the original Bai's algorithm). These parameters must be selected under strict geomechanical criteria given the stress conditions and the rock mass quality where the stope will be built.

In terms of regularity of the stope design obtained by the IP formulation, we can see a great improvement in all the instances shown compared to Bai's algorithm. This will ensure an easier work for the production and construction phase in-field. However, the final stope design could still be modified in real life work given the blasting control and the presence of joints or other structures.

The stope design could be further regularized using the same convexity constraints structure, but with different coordinates. For instance, in the cylindrical coordinate system, we could take rings instead of columns: the group of blocks with same $r$ and $z$ coordinate, but different $\theta$. If we apply the same restrictions but changing these coordinates, we will avoid the irregularities not only vertically, but horizontally as well. This regularization will improve the stope geometry, but it will worsen the stope profit, therefore, the decision to include these new constraints will depend on the mining engineer. As a downside, adding these new constraints would increase the variables and restrictions notably, and the instances shown are already remarkably large.

Despite the low resolution times for these big instances, the definition of the instance using Gurobi requires a large amount of RAM. This is a problem in some cases, where the sole definition of variables and restrictions in Gurobi consumes all the available RAM. This is not an issue with the network structure used by Bai et al. (2013a) since it is more compact, requiring less memory to be defined and solved. However, these big instances are not common in Sublevel Stoping given its

selective nature. Admittedly, this issue could become a problem when multiple stopes have to be optimized simultaneously as in Bai et al. (2014).

A possible alternative to reduce the size of the instance would be the implementation of a heuristic that, instead of applying the convexity constraints in every column of the block model, focus only in its outer columns, controlled by a parameter $\rho$ defined from the initial raise. From $r > \rho$, this heuristic would apply the convexity constraints, leaving the inner part of the block model without these restrictions. This would take advantage of the fact that the inner parts of the block model does not present convexity issues. This heuristic could achieve good results faster than the IP-formulation and it would work with larger instances.

A usual issue in stope optimization is avoiding stope overlapping when multiple stopes are considered. Bai's formulation explicitly avoids this issue defining a single raise for each stope, and a different cylindrical coordinate system for each one of them, where each block of the original block model belongs only to one of these systems, as it is shown in Bai et al. (2014). Since the convexity constraints are applied to each one of these different coordinate systems, the IP-formulation does not generate overlapping stopes.

Finally, regarding runtimes, the IP-formulation is slower than the network structure solving the same instances, and the addition of convexity constraints increases the runtimes even more. However, this formulation remains remarkably fast for this kind of problems: the stope design definition problem belongs to the strategic mine planning stage, where decisions takes months or years to be made, so fast runtimes are not mandatory. For this reason, the IP-formulation with convexity constraints could be used in real-life applications.

## 5 Conclusions

The proposed methodology allows the determination of optimal stope designs, fulfilling geomechanical requirements. It generates feasible stopes in disseminated orebodies, avoiding unstable and irregular geometries. The designs comply with technical requirements such as the stope drilling pattern. The formulation can be solved in reasonable times for real life cases, and it can be extended to allow further regularization of stope design or faster resolution times using heuristics.

**Acknowledgments** The Government of Canada provided a Research Scholarship to the first author. The authors are grateful for the comments, corrections and insights made by the three anonymous reviewers.

## References

Alford C (1996) Optimisation in underground mine design. In: Proceedings of 25th APCOM. AusIMM, Melbourne, pp 213–218

Ataee-Pour M (2000) A heuristic algorithm to optimise stope boundaries. PhD Thesis, University of Wollongong

Ataee-Pour M (2005) A critical survey of the existing stope layout optimization techniques. J Min Sci 41:447–466

Bai X, Marcotte D, Simon R (2013a) Underground stope optimization with network flow method. Comput Geosci 52:361–371
Bai X, Marcotte D, Simon R (2013b) Incorporating drift in long-hole stope optimization using network flow algorithm. In: Proceedings of 36th APCOM. APCOM, Porto Alegre, p 391–400
Bai X, Marcotte D, Simon R (2014) A heuristic sublevel stope optimizer with multiple raises. SAIMM 114:427–434
Bieniawski Z (1989) Engineering rock mass classifications: a complete manual for engineers and geologists in mining, civil, and petroleum engineering. Wiley, New York
Cheimanoff N, Deliac E, Mallet J (1989) GEOCAD: an alternative CAD and artificial intelligence tool that helps moving from geological resources to mineable reserves. In: 21st Application of computers and operations research in the mineral industry: 21st international symposium: papers, p 471
Coulomb CA (1776) Essai sur une application des regles des maximis et minimis à quelquels problèmes de statique relatifs a l'architecture. Mem Acad Roy Div Sav 7:343–387
Crouch S, Starfield A (1983) Boundary element methods in solid mechanics. George Allen and Unwin, London
Hoek H, Carranza-Torres C, Corkun B (2002) Hoek–Brown failure criterion—2002 edition. In: Proceedings of the fifth North American rock mechanics symposium (NARMS-TAC). University of Toronto Press, Toronto, p 267–273
Lane K (1988) The economic definition of ore: cut-off grades in theory and practice. Mining Journal Books, London
Laubscher DH (1990) A geomechanics classification system for the rating of rock mass in mine design. J S Afr Inst Min Metall 90:257–273
Lerchs H, Grossmann I (1965) Optimum design of open-pit mines. Trans CIM 58:47–54
Manchuk J, Deutsch C (2008) Optimizing stope designs and sequences in underground mines. SME Trans 324:67–75
Mathews KE (1980) Prediction of stable excavation spans for mining at depths below 1000 m in hard rock. Report to Canada Centre for Mining and Energy Technology (CANMET), Department of Energy and Resources
Ovanic J, Young D (1995) Economic optimisation of stope geometry using separable programming with special branch and bound techniques. In: Third Canadian conference on computer applications in the mineral industry, p 129–135
Picard J (1976) Maximal closure of a graph and applications to combinatorial problems. Manag Sci 22:1268–1272
Riddle J (1977) A dynamic programming solution of a block-caving mine layout. In: Application of computer methods in the mineral industry: proceedings of the fourteenth symposium, p 767–780
Sandanayake D, Topal E, Ali Asad M (2015) A heuristic approach to optimal design of an underground mine stope layout. Appl Soft Comput 30:595–603
Topal E, Sens J (2010) A new algorithm for stope boundary optimization. J Coal Sci Eng 16(2):113–119